Desalination and Water Treatment
www.deswater.com
doi: 10.5004/dwt.2023.30209

316 (2023) 395–407
December

Nickel(II) adsorption in aqueous solutions with cost-effective mesoporous *Bitlis pumice* stone

Serhat Yamaç[a], Sinan Mehmet Turp[b,*], Hakan Çoban[c]

[a]*Department of Emergency and Disaster Management, Bitlis Eren University, Rahva Campus, Bitlis 13100, email: serhatymc13a@gmail.com*
[b]*Department of Chemistry and Chemical Processing Technologies, Bitlis Eren University, Tatvan, Bitlis 13100, email: smturp@beu.edu.tr*
[c]*Department of Civil Engineering, Bitlis Eren University, Rahva Campus, Bitlis 13100, email: hcoban@beu.edu.tr*

Received 18 May 2023; Accepted 5 December 2023

ABSTRACT

In this study, comprehensive analysis was performed on natural pumice stone from the Bitlis region of Eastern Anatolia with regard to the removal of nickel(Ni). In terms of various calculation models involving textural parameters (e.g., surface area, pore volume, particle size), the surface area of the *Bitlis pumice* samples obtained was 1.3491 m^2/g Brunauer–Emmett–Teller model, 1.3719 m^2/g Barrett–Joyner–Halenda model, and 16.0137 m^2/g Langmuir model, whereas, the particle size was 4,447 nm. Fourier-transform infrared spectroscopy analysis also showed that in the region of 1,200–950 cm^{-1} there was a band (and shoulder) of symmetric and asymmetric stretching of the Si–O–Si bond. Accordingly, based on the kinetic, equilibrium, and thermodynamic studies of Ni(II) adsorption by *Bitlis pumice* from aqueous solutions, in order not to affect the heavy metal activation in the adsorption of Ni heavy metal with *Bitlis pumice*. Experiments were carried out at pH 7, using 1 g of pumice and 120 min at an input concentration of 3 mg/L Ni. 99% removal was achieved during contact time. The best removal efficiency of Ni(II) (99%) was obtained with an adsorbent dosage of 3 mg/L, pH 7 with a contact time of 120 min. This involved the use of the Langmuir isotherm model (R^2 = 0.99). These processes were interpreted chemically with the use of the second-order pseudo-kinetic model (R^2 = 0.99).

Keywords: Bitlis pumice; Nickel(II) adsorption; Heavy metal removal; Pumice adsorbent

1. Introduction

The use of appropriate adsorbents and adsorption methods providing the cheapest, most easily available and most readily applicable, with the highest uptake and the least complex way to extract toxic heavy metals from wastewater, are of prime importance for a clean ecosystem and human health [1]. Despite efforts to incorporate new methods of discharge of heavy metals, the removal of toxic metals remains a serious problem facing modern society. Nickel(II) is a very important heavy metal in this context, as are lead (Pb), zinc (Zn), mercury (Hg), cadmium (Cd), copper (Cu), chromium (Cr), and arsenic (As). Ni(II) causes toxic damage to humans (such as allergic reactions, chronic bronchitis, and cancer of the lung and nasal sinus) [2–6], and the creation of green and blue environments (*via* industrial wastewater, contaminated soils and sediments of lateritic and sulfidic Ni(II) deposits associated with mafic-ultramafic rocks [7,8]. Since it is a widely used heavy metal in industry (e.g., in the manufacture

* Corresponding author.

of stainless steel, alloys, special steels, coatings, electric batteries, and electroplating) and it commands a high market price, the recycling of Ni(II) is economically profitable [9]. Accordingly, several adsorbent materials in the form of natural and synthetic chemicals and composites, have been used to prevent Ni(II) pollution (e.g., biofilm placed) zeolite [10], natural kaolinite, nano- and surfactant-coated alumina [11,12], *Calotropis procera* [13], carbon nanotubes [14,15], chitosan-coated PVC beads [16], apricot stone [17,18], protonated rice bran [19], orange peel, eggshell waste [20], bamboo activated carbon [21], waste pea shell [22], olive stone [23], Remazol black B-sulfonamide polymeric resin [24], calcium carbonate coated bacterial magnetosomes [25], mineral–organic hybrid adsorbents [26], and raw and modified plant wastes [27]. On the other hand, research into the modified or unmodified uses of natural pumice - a light and inexpensive material with high porosity - as an adsorbent in toxic heavy metal (e.g., Cd, Cu, Zn, Pb, Cr) extraction, have been of great interest in the last decade [28–41]. Specifically, there has been interest in the adsorption capacity of natural pumice which depends on several textural parameters such as surface area, pore volume, pore size, and particle size [42], and its surface morphology, cellular texture, and vesicular structure, all of which make it an appropriate adsorbent material [36,43,44].

In this respect, the study carried out for this purpose is a very important and innovative research point for the elimination of nickel pollution from water. Eliminating the nickel pollution by using *Bitlis pumice*, one of the volcanic rocks of the same region, is another innovative part of the study in terms of creating a different environmental cycle. Within the context of this comprehensive analytical study involving *Bitlis pumice*, its efficiency as a form of adsorbent in the purification quality of Ni(II). This is based on physical adsorption studies and thermodynamic applications: scanning electron microscopy (SEM), textural and physical adsorption analyses, Fourier-transform infrared spectroscopy (FTIR), thermogravimetric analysis (TGA), chemical analysis of Ni-bearing contaminated water, isotherm, kinetic and thermodynamic studies of heavy metal adsorption, removal efficiency, effects of contact time, initial ion concentration of pH, and temperature.

2. Materials and methods

2.1. Experimental materials

A UV-spectrophotometer (WTW 7600 UV-VIS) was used for adsorption measurement purposes. All shaking operations were done using a magnetic stirrer (2 mag magnetic motion-mix 15 eco) model shaker. Ni(II) (Merck, Darmstadt, Germany) solution and adsorbent weighing were measured with the use of Ohaus Adventurer Pro brand precision scales. The Ni(II) was made with deionized water (ELGA PURELAB Option DV-25) in a dilution of stock solution and initial dyestuff concentrations.

2.2. Adsorbent

The *Bitlis pumice* (38°38′03.0″N 42°26′10.3″E, Bitlis, Eastern Türkiye) sample was cleaned and dried.

2.3. Artificial wastewater

Nickel salt (Merck, Germany), which is prepared from a 1,000 mg/L stock solution of Ni(II) heavy metal salt at concentrations of 1, 3, and 5 mg/L, is an aqueous solution. The adsorption study of heavy metals is carried out in a laboratory environment. All aqueous solutions are prepared using a deionized water device (ELGA PURELAB Option-Q).

2.4. Experimental methods

Adsorption experiments were performed with contact times of 10, 30, 60, and 120 min for each concentration, along with 0.5, 1, and 5 g of adsorbent material. For each initial concentration (1, 3, and 5 mg/L), 0.5, 1, and 5 g of *Bitlis pumice* were added, and the adsorption process was carried out separately for the 4 different contact times. Ni(II) removal was conducted using a magnetic stirrer (2 mags magnetic motion-mix 15 eco) at 500 rpm in a 50 mL beaker. Samples were placed in falcon tubes and prepared for analysis. The experimental samples obtained were measured using the atomic absorption spectroscopy device. The initial concentration, amount of adsorbent, and contact time removal efficiencies, were calculated. In addition, to provide more detailed information about the adsorption process, the adsorption isotherm, kinetics and thermodynamics were calculated and interpreted.

2.5. Bitlis pumice characterization studies (SEM, physical adsorption, FTIR, and TGA analyses)

SEM is an electron microscope that obtains an image by scanning the sample surface using a focused beam of electrons. In this study, the characterization study of *Bitlis pumice* was performed the in DAYTAM Laboratory using the Zeiss Sigma 300 device. Brunauer–Emmett–Teller (BET) surface analysis, Barrett–Joyner–Halenda (BJH), Langmuir (LA) models, with regard to textural properties such as specific surface area, pore volume, pore size, and particle size of the studied pumice sample were determined using various calculation models from the N_2 adsorption–desorption isotherms at 76 K using Micromeritics 3Flex equipment. About 0.37 g of the sample was placed in a glass tub to be degassed and analyzed. The cold and warm free space was 63.9213 and 18.6914 cm^3, respectively. The analytical results of the physical adsorption models (BET, LA, and BJH) were obtained automatically from the Micromeritic device. The FTIR analysis of the *Bitlis pumice* was done in the YUMERLAB (Yalova University) laboratory using the PerkinElmer Spectrum 100 device, and the TGA analysis of the *Bitlis pumice* was performed using the Seiko TG/DTA 6300 device.

2.6. Adsorption studies

Adsorption is considered one of the most effective methods for removing a wide variety of pollutants, whose application has spread to wide areas [67–78].

The adsorption removal results obtained from the experiments were calculated using the yield Eq. (1).

$$\text{Heavy metal adsorption } \% = \left(\frac{C_0 - C_e}{C_0} \right) \quad (1)$$

where C_e is the heavy metal concentration (mg/L) at equilibrium and C_0 is the initial heavy metal concentration (mg/L).

2.7. Isotherm and kinetics analysis

Langmuir, Freundlich, Temkin and Dubinin–Radushkevich models were used to fit the experimental data and determine the most appropriate isotherm model [45].

Adsorption data of Ni(II) heavy metals on *Bitlis pumice* were investigated using the Langmuir (2), Freundlich (3), Temkin (4), and Dubinin–Radushkevich (5) isotherms with the help of Eqs. (2)–(5).

$$\frac{C_e}{q_e} = \left(\frac{1}{q_{\max} K_L}\right) + \left(\frac{C_e}{q_{\max}}\right) \tag{2}$$

$$\ln q_e = \ln K_F + \left(\frac{1}{n}\right) \ln C_e \tag{3}$$

$$q_e = \beta \ln a + \beta \ln C_e \tag{4}$$

$$\ln q_e = \ln X_m - K\varepsilon^2 \tag{5}$$

Kinetic studies are required for the design of the adsorption process. Adsorption rate constants should be calculated to determine the time required for the removal of the components that must be adsorbed in order to maximize the adsorption efficiency. Two different kinetic models were used in the experimental series in which the *Bitlis pumice* is used as an adsorbent material for the removal of Ni(II) from the artificial water. The linearized equation of the pseudo-first-order and pseudo-second-order is represented by Eqs. (6) and (7):

$$\log\left(q_e - q_t\right) = \log q_e - \left(\frac{k_1 t}{2.303}\right) \tag{6}$$

$$\frac{1}{q_t} = \frac{1}{k_2 q_e^2} + \left(\frac{1}{q_e}\right) t \tag{7}$$

Thermodynamic parameters reflect the suitability of the adsorption process under constant pressure and temperature. It is essential to calculate the thermodynamic parameters to conclude the adsorption process. This process gives information as to whether the process is spontaneous or endothermic/exothermic [46].

Equilibrium constants obtained under different test conditions are calculated with the use of Eq. (8).

$$\ln b = \frac{\Delta S}{R} - \frac{\Delta H}{RT} \tag{8}$$

3. Results and discussion

3.1. Nature of Bitlis pumice

Pumice is a product of explosive volcanic eruptions once gases are released during the solidification of silica-rich molten lava during cooling as a form of its vesicular structure (Fisher et al. 1984). The pumice stone contains approximately 70% voids [47] with an average porosity of 90%, and it floats on water due to its low density [43,48]. Although pumice has a sponge-like texture, and a vesicular structure with high porosity, typically there is no interconnection between the pores. This fact causes the pores to form in visibly numerous microscopic sizes (Fig. 1). It possesses an amorphous (glassy) crystal structure and a low surface area of ≈ 5 m^2/g, in which there is a broad distribution of pores of varying size, and the absence of volume fractality [48,49]. It is light due to the vesicles inside it. Different structural locations of pumice have different elemental compositions that affect its adsorption capability [49]. Researchers have described the two types of pumice as silica-rich light-colored acidic and silica-poor dark-colored basic. Indeed, in the volcanology literature, the term 'basic pumice or basaltic pumice' corresponds to dark-colored silica-poor 'scoria' and differs from the other form of pumice in that it has denser and larger vesicles with thicker pore walls [50].

The silica-rich white pumice used in this study is a product of the well-known explosive Nemrut stratovolcano in the Bitlis region of Eastern Anatolia [51], which has 70% of Turkey's reserves of pumice. The average chemical composition [51] and density of *Bitlis pumice* used in this study are given in Table 1. It contains a high percentage of silica (75 wt.%), and moderate amounts of aluminum (12.3 wt.%) making up its aluminosilicate composition. Moreover, it is also significantly low in potassium, sodium, and iron,

Fig. 1. Silica-rich acidic *Bitlis pumice*.

while the percentages of calcium and magnesium are even lower (Table 1). Notably, Liu et al. [52] and Çiftçi & Meriç [35] emphasized that high contents of silica in pumice cause a negative charge on its surface, meaning that it could easily adsorb heavy metals.

Fig. 2 shows SEM images of the surface morphology and crystal structure of the *Bitlis pumice*. The image shows a pattern of highly porous and irregular vesicular texture containing large cavities. In addition, amorphous crystal intra-structures of *Bitlis pumice* of regular surface morphology demonstrate suitable sites for adsorption.

3.1.1. FTIR analyses of Bitlis pumice

FTIR for *Bitlis pumice* is presented in Fig. 3. In the region of 1,200–950 cm^{-1} there is a band (and shoulder) where the pumice has symmetric and asymmetric stretching of the Si–O–Si bond (from the present amorphous SiO_2 in pumice). In the region of approximately 780 cm^{-1} the band of plane deformation vibrations which are formed in symmetric and asymmetric forms corresponds to (rocking and scissoring) corresponding to the Si–O bond (from the present amorphous SiO_2 in pumice). The band at 1,629 cm^{-1} is the result of the presence of water molecules in the sample. The bands in the range of 2,850–3,000 cm^{-1} result from the water and the presence of hydroxyl groups in the pumice sample.

3.1.2. TGA analysis of Bitlis pumice

As can be seen in Fig. 4, exothermic entry starts at 180°C. In addition, at these temperature at 180°C leaves its water slowly.

3.1.3. Textural aspects

Textural properties in the form of surface area, pore volume, pore size, and particle size of the studied *Bitlis*

Table 1
Major elements compositions (wt.%) of the *Bitlis pumice* (Schmincke et al. 2014)

Sample	Locality	Rock	Color	Density	Major elements (wt.%)											
No				g/cm^3	SiO_2	Al_2O_3	CaO	Fe_2O_3	K_2O	Na_2O	MnO	MgO	P_2O_5	TiO_2	SO_3	LOI
5_KPO	*Bitlis*	*pumice*	White	1.00	72.5	12.3	0.33	2.14	4.66	4.79	0.05	0.08	0.01	0.14	0.06	3.29

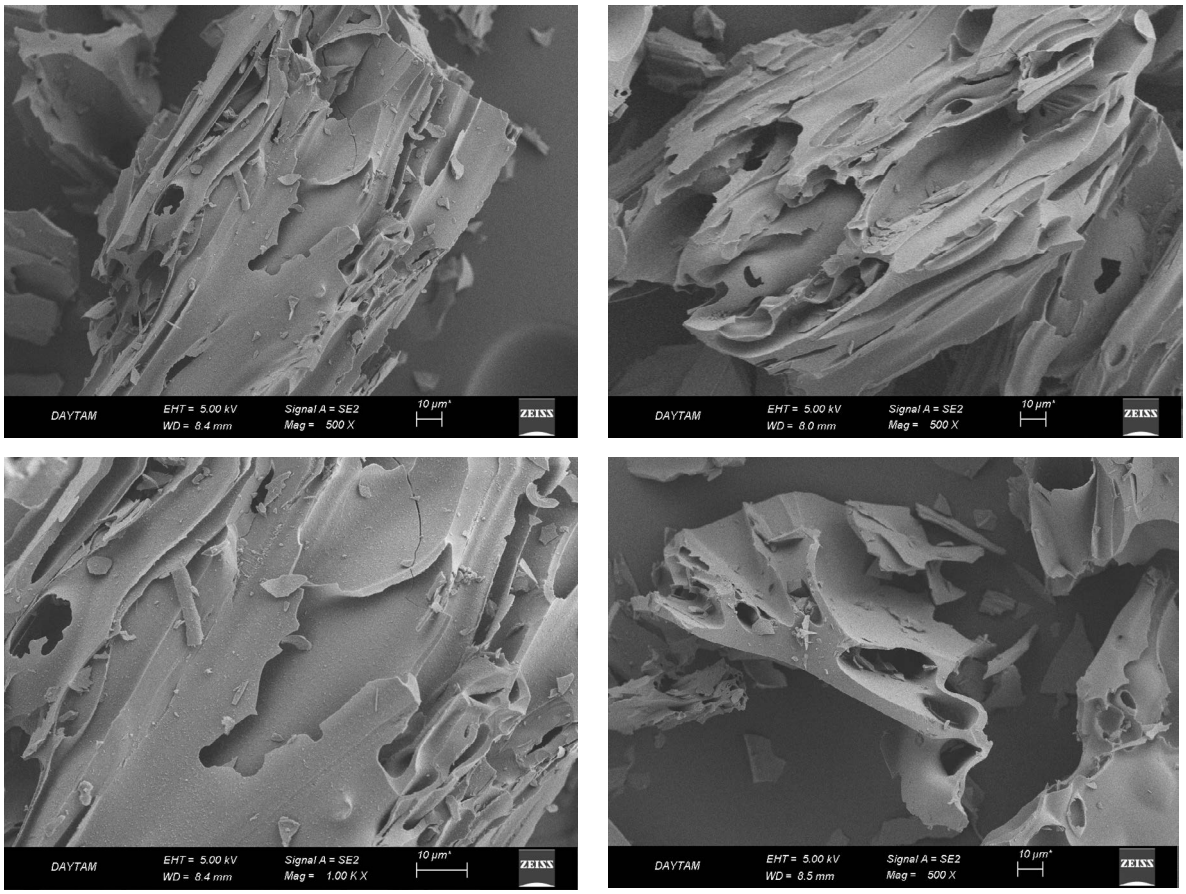

Fig. 2. Scanning electron microscopy image of *Bitlis pumice*.

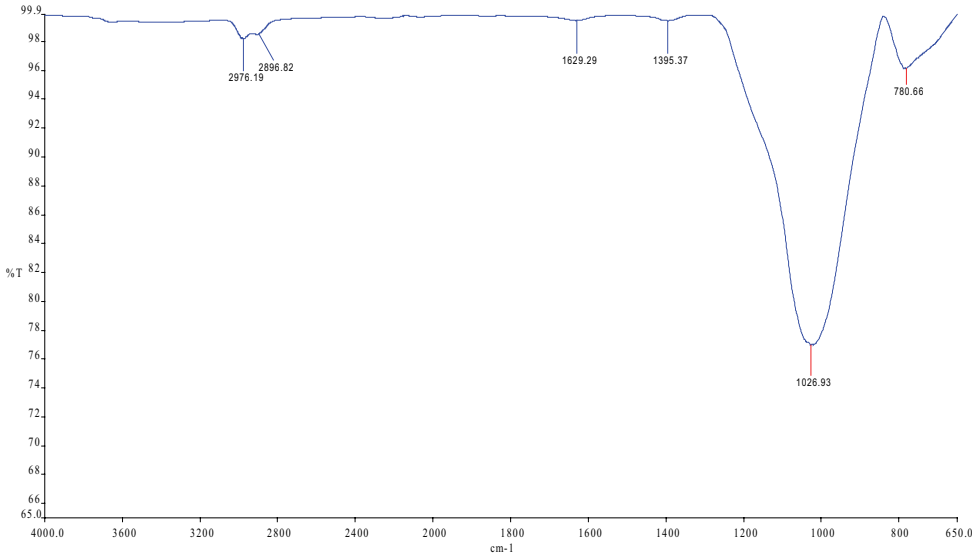

Fig. 3. Fourier-transform infrared spectra of *Bitlis pumice*.

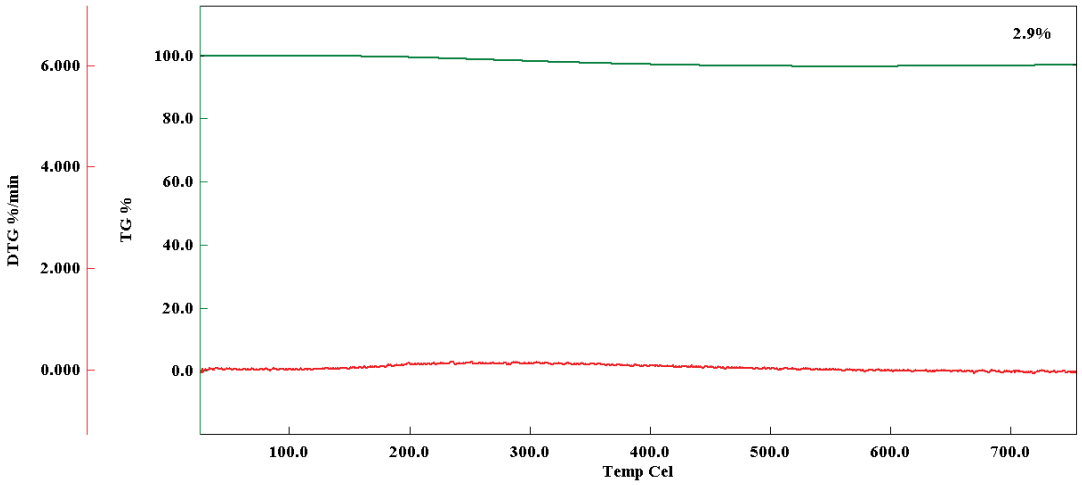

Fig. 4. Thermogravimetric analysis of *Bitlis pumice* (temperature range between 25°C and 750°C).

pumice sample were measured by the physical adsorption method at low pressures with high resolution. As a result of the experiments, the "adsorption–desorption isotherm" was obtained, which is presented in Fig. 5.

The typical three stages of the isothermal adsorption curves of the *Bitlis pumice* sample, showing similarity to those of Harrat (Madina, Saudi Arabia) pumice (Alraddadi and Assaedi [42]), as can be seen in Fig. 5 [42]. At Stage 1, before point B (single point surface area at P/P^0 = 0.28 on the adsorption curve), adsorption of the first layer of the N_2 molecules occurred on the solid surface. At Stage 2, multi-layer adsorption of the N_2 molecules forms, and the number of adsorbed layers (hence the adsorption capacity) progressively increase with the increasing relative pressure. At the last stage (Stage 3, elevated vertical stage), the adsorption pressure progressively increases the saturated vapor pressure of the gas, and the nitrogen molecules cause liquification and the capacity achieves its maximum adsorption value. The pressure is then decreased, and the nitrogen progressively begins to desorb. The adsorption quantity of nitrogen at Stage 1 is <0.5 and <1 cm^3/g at Stage 2, while at Stage 3 the maximum adsorption quantities are in the range of 2.7035–8.8635 cm^3/g (Fig. 3).

Accordingly, the BET, LA, and BJH models are used to calculate the textural parameters from the experimental isotherms of the *Bitlis pumice* sample. These are presented in Table 2 and compared with those of Harrat pumice [42]. In the case of the *Bitlis pumice* sample, the BET surface area was obtained as 1.3491 m^2/g, which is lower than that of the Harrat pumice sample (1.6698 m^2/g, Table 1). The *Bitlis pumice* sample's single-point surface area (B, Fig. 3) at P/P^0 = 0.28 was observed as 1.1241 m^2/g, which is close to that of the BET surface area (Table 5). The Langmuir surface area (based on a monolayer assumption) was obtained as 16.0137 m^2/g, which is much higher than that of the Harrat sample (2.2360 m^2/g). In the case of the *Bitlis*

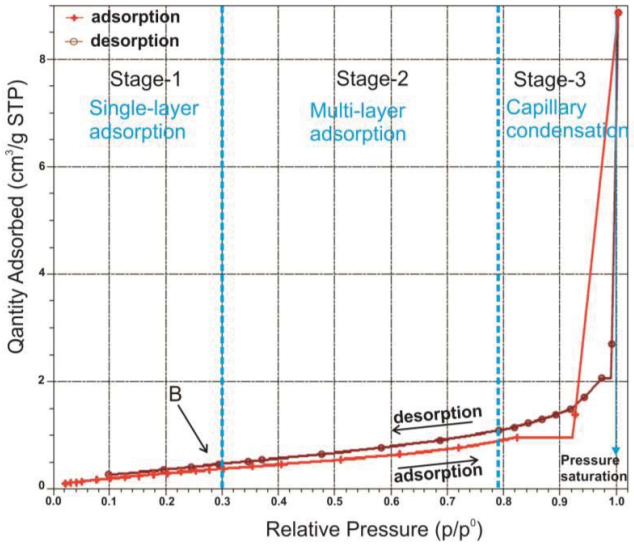

Fig. 5. Experimental nitrogen adsorption–desorption isotherms of *Bitlis pumice*, indicating the different adsorption stages.

pumice, the single point total pore volume of the pores with a diameter width less than 40.3122 nm at P/P^0 = 0.950000000 was 0.002126 cm^3/g, which is lower than that of the Harrat pumice (with a diameter less than 77.9710 nm at P/P^0 = 0.974531650 is 0.00334 cm^3/g).

The BJH adsorption cumulative surface area and pore volume of the *Bitlis pumice* sample were respectively 1.3719 m^2/g and 0.002022 cm^3/g (Table 2). The BJH surface area of the *Bitlis pumice* was higher than its BET surface area. Similarly, the particle size of the *Bitlis pumice* sample was obtained as 4,447 nm, which was higher than that of the Harrat pumice sample (3,593 nm, Table 2). Therefore, the specific surface area and particle size are important factors in determining the efficacy of the rock in several applications. To illustrate, it increases the surface area of particles and their ability to adsorb by making the material susceptible to applications such as water purification [43]. Hence, decreasing particle size increases the surface area, and the adsorption capacity of the smaller particles becomes higher as they become more reactive. This is because trace elements tend to be concentrated in the finer particles. Accordingly, Figs. 6 and 7 show the BET surface area vs. particle size and

Table 2
Textural properties of *Bitlis pumice* (sample 5_KPO), and comparison with those of the Harrat Khayra pumice (sample S2, [43])

		Bitlis	Harrat
Textural	Sample No#	5_KPO	S2
Parameters	Method		
Surface area (S)	Brunauer–Emmett–Teller surface area (m^2/g)	1.3491	1.6698
	Single point surface area (m^2/g)	1.1241	1.6489
	Langmuir surface area (m^2/g)	16.0137	2.236
	t-plot external surface area (m^2/g)	2.1332	1.0618
	Barrett–Joyner–Halenda adsorption cumulative surface area of pores diameter (m^2/g)	1.3719	0.763
	Barrett–Joyner–Halenda desorption cumulative surface area of diameter (m^2/g)	1.8353	0.7376
Pore volume (V_p)	Single point adsorption total pore volume of pores	0.002126	0.00334
	(less than 40.3122 nm diameter at P/P^0 = 0.950 000 000 cm^3/g)		
	Barrett–Joyner–Halenda adsorption cumulative volume of pores (cm^3/g)	0.002022	0.00616
	Barrett–Joyner–Halenda desorption cumulative volume of pores (cm^3/g)	0.004222	0.00625
Pore size (dav)	Adsorption average pore width (4 V S.1 by Brunauer–Emmett–Teller)	6.3022	7.9877
	Barrett–Joyner–Halenda adsorption average pore diameter (4 V S.1) (nm)	5.8952	32.318
	Barrett–Joyner–Halenda desorption average pore diameter (4 V S.1) (nm)	9.2015	33.911
Nano particle size	Average particle size (nm)	4,447.4	3,593.2

*less than 77.9710 nm diameter at P/P^0 = 0.974 531 650 (cm^3/g)

Table 3
Comparison of initial concentration, adsorbent dose, removal efficiency parameters with different adsorbents (120 min, contact time, pH: 7, 20°C)

Adsorbent	Ni(II) (mg/L)	Dose (g/L)	q_{max} (mg/g)	References
Rice husk ash	100	1	4.84	[68–79]
Manganese dioxide	10–200	10	114.9	[69–80]
Activated carbon	29.3	0.4	34.04	[70–81]
Montmorillonite	50–500	0.5	100%	[71–82]
Manganese oxide coated zeolite	100	1	7.9	[72–83]
Bitlis pumice	3	1	149.9	This study

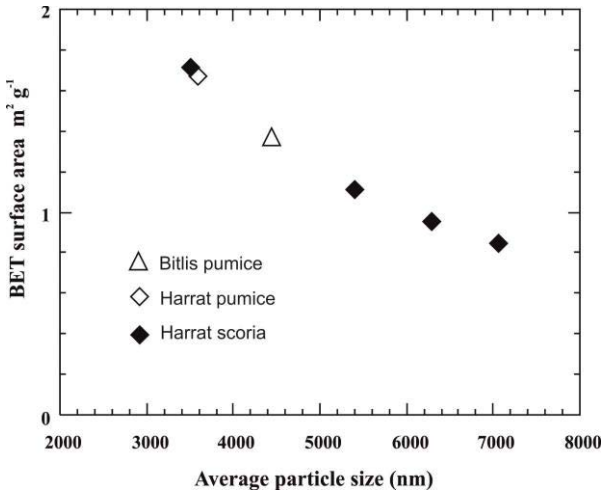

Fig. 6. Correlation between Brunauer–Emmett–Teller surface area (m^2/g) and average particle size (nm) for *Bitlis pumice*, Harrat pumice, and scoria samples.

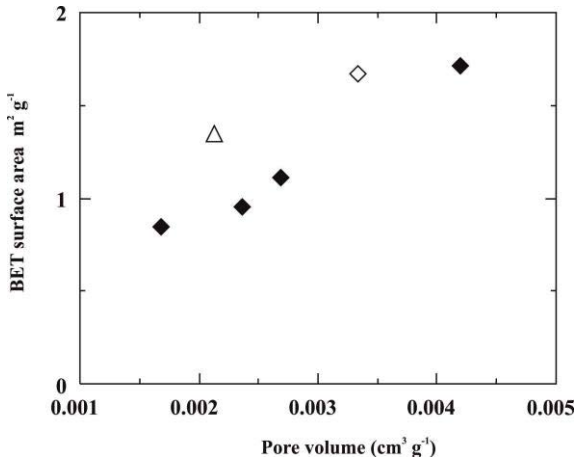

Fig. 7. Correlation between Brunauer–Emmett–Teller surface area (m^2/g) and pore volume (cm^3/g) for *Bitlis pumice*, Harrat pumice, and scoria samples.

pore volume variations for the *Bitlis pumice*, the Harrat pumice and the scoria samples. The surface area increases with decreasing particle size, while it expands with increasing pore volume. These variations in particular make the adsorption capacity of the *Bitlis pumice* more suitable for water purification. Considering the average adsorption pore width of the *Bitlis pumice* (6.3022 nm), like the mesoporous structure of the Harrat pumice (7.9877 nm), the structure of *Bitlis pumice* could be classified as mesoporous material (ranging between 2 and 50 nm) according to the conventions of International Union of Pure and Applied Chemistry (IUPAC) (Thommes et al. [55]). This indicates its low density [42,53]. This fact also suggests that the channels and cavities of the mesoporous *Bitlis pumice* can selectively separate ions and molecules according to their different sizes [42,54,55].

3.1.4. Initial effects of Ni(II) heavy metal concentration on adsorption

The initial heavy metal concentration in aqueous solutions significantly affected the adsorption process. This effect depends on the type of heavy metal, the presence of cations and groups on the surface of the adsorbent affecting the ability of the surface to bind metal ions. For example, during the waste tea bed adsorption experiment, the adsorbent material rapidly achieved the saturation process at 200 mg/L Ni(II) throughout the initial concentration [45]. The results that are obtained in the adsorption experiments with regard to Ni(II) heavy metal at 1, 3, and 5 mg/L initial concentrations with 1 g *Bitlis pumice* are as shown in Fig. 8. The adsorption efficiency is increased in parallel with the increase in heavy metal concentration. The total saturation of the adsorbent then occurred at a maximum concentration of 3 mg/L Ni(II) heavy metal (Table 3).

3.1.5. Effects of adsorbent on Ni(II) heavy metal adsorption

The results of the experiments that was carried out to determine the effect of the amount of *Bitlis pumice* on the

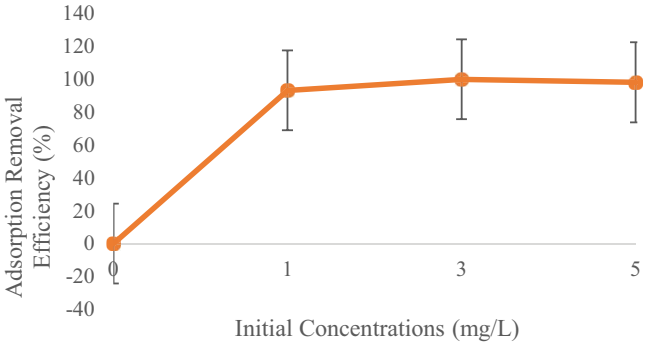

Fig. 8. Effect of initial concentration on the adsorption of *Bitlis pumice* (1 g *Bitlis pumice*, 120 min contact time, pH: 7, temp.: 25°C).

adsorption of the heavy metal Ni(II) are given in Table 4. When the *Bitlis pumice* amount is increased to 0.5 g, the amount of heavy metal adsorption also increases and reaches equilibrium. The best yield that was obtained in the experiment was 99% with regard to 1 g *Bitlis pumice* (Fig. 9).

As a result of the experiments that was carried out to determine the effect of different MHLT-KTS amounts on the adsorption of Cr(VI) on MHLT (magnetic halloysite nanotubes)-KTS (biopolymeric chitosan) nanocomposite, the optimum amount of MHLT-KTS nanocomposite was shown to be 150 mg (6 g/L MHLT-KTS) [46]. In addition, the adsorption capacity of a local clay variety (BM-Clay2) at an initial concentration of 50 mg/L via constant Ni(II), which varies from 0.2 to 5 g/L was investigated. After the adsorbent dose reached the highest removal efficiency at 3 g/L, the efficiency started to decrease. This was explained by the fact that the concentration of metal ions in the solution reached a low value, and the adsorption driving force was minimal [59].

3.1.6. Effect of contact time on Ni(II) heavy metal adsorption

The adsorption performances of *Bitlis pumice* were tested with the use of batch adsorption experiments. It was

Table 4
Comparison of pH and contact time with *Bitlis pumice* and different adsorbents

Adsorbent	pH	Time (h)	References
Rice husk ash	2–10	5	[79]
Manganese dioxide	4.5–7.5	24	[80]
Activated carbon	2.5–8.0	48	[81]
Montmorillonite	3–11	24	[82]
Manganese oxide coated zeolite	3–8	0.5	[83]
Bitlis pumice	2–11	2	This study

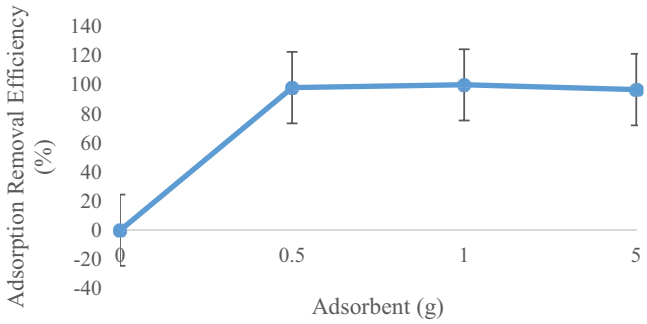

Fig. 9. Effect of adsorbent amount on the adsorption of *Bitlis pumice* (3 mg/L Ni(II) heavy metal concentration, 120 min contact time, pH: 7, temp.: 25°C).

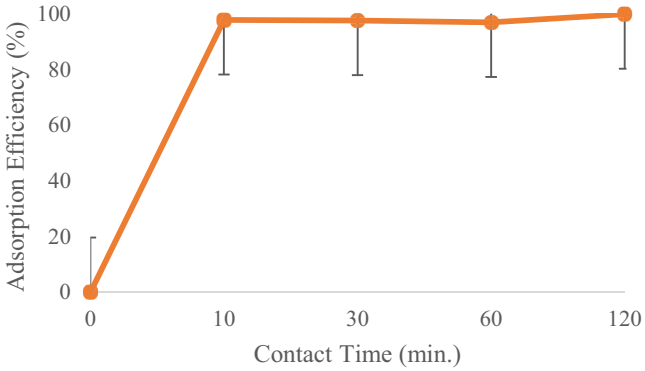

Fig. 10. Effect of contact time on the adsorption of *Bitlis pumice* (3 mg/L Ni(II) heavy metal concentration, pH: 7, 1 g adsorbent material, temp.: 25°C).

observed that equilibrium was achieved in the first 10 min of the adsorption process. This can be explained by the high number and availability of active sites, along with the driving force required for the transfer of the heavy metal Ni(II) onto the pumice used in the experiment [56–66]. However, the fact that the adsorption curve changed very little in the later stages of the experiment is attributed to the limited amount of the heavy metal because it reached the active sites in the pumice pores very rapidly. The adsorbent achieved equilibrium in the first 10 min of the 120-min adsorption period, and the highest removal efficiency (99%) was also obtained within 120 min (Fig. 10, Table 5).

It is therefore observed that there was not a significant Ni(II) removal indication obtained at 20°C in the case of both pumice and magnetic iron-coated pumice within a 12-h adsorption time. This fact is also verified in former Ni(II) removal studies. Using MnO_2 in Ni(II) results in change because of the removal processes that continued for up to 24 h [57]. Moreover, a maximum of 97.75% removal was achieved in 120 min in the Ni(II) removal study using modified waste newspaper [58].

3.1.7. pH effect

In the adsorption process, the pH value, which affects the metal binding sites and metal chemistry of the adsorbent surface, is a crucial control parameter. To detect its effect on the removal of Ni(II) ions, experiments were carried out at different pHs at an inlet concentration of 5 mg/L in terms of the greatest removal efficiency. The maximum Ni(II) removal efficiency using *Bitlis pumice* was obtained at pH = 7 (Fig. 11, Table 5).

While the adsorption capacity decreases due to high solubility at a low pH, an increase in pH causes growth in the removal of nickel ions [58]. This is because efficiency decreases largely for H^+ ions while competing with Ni(II) ions within active sites due to low pH levels [59].

3.1.8. Temperature effect

In adsorption experiments, the temperature is directly related to the kinetic energy levels of the metal ions in the

Table 5
Adsorption isotherm constants for *Bitlis pumice*

Langmuir isotherm constants	Freundlich isotherm constants	Temkin isotherm constants	Dubinin–Radushkevich isotherm constants
q_m (mg/g) = 0.145	K_F (mg/g) = 2.325	B (J/mol) = 0.1432	X_m (mg/g) = 1.93
K_L (L/mg) = 0.00027	n (g/L) = 135.13	A_t (L/g) = 1.007	K (mol²/J²) = 10
R^2 = 0.99	R^2 = 0.90	R^2 = 0.91	R^2 = 0.87

solution. An increase in temperature may cause a growth in the diffusion rate of the adsorbate. The higher affinity of the adsorbent for metal, along with the increase in the active sites of the adsorbate, can often facilitate the adhesion of heavy metals to the surface by further increasing their uptake. In most cases, room temperature is preferred for the determination of adsorption capacity. This is because the operating cost of the experiment increases at high temperatures [60,61].

Experiments involving temperature on the adsorption of *Bitlis pumice* on heavy metal Ni(II) with a 5 mg/L initial concentration were conducted along with the 3 g adsorbent and pH: 7–8 levels for 120 min contact time. It can be seen in Fig. 12 that the best removal efficiency in the adsorption process is 96% at 15°C, while the optimum temperature is determined to be 20°C.

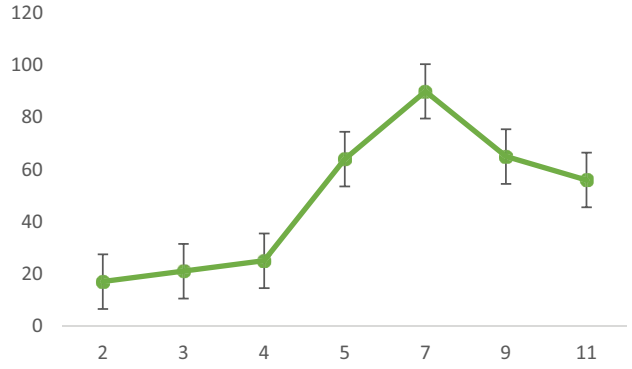

Fig. 11. pH effect on the adsorption of *Bitlis pumice* (3 mg/L Ni(II) heavy metal concentration, 120 min, contact time, 5 mg/L initial concentration, temp.: 25°C).

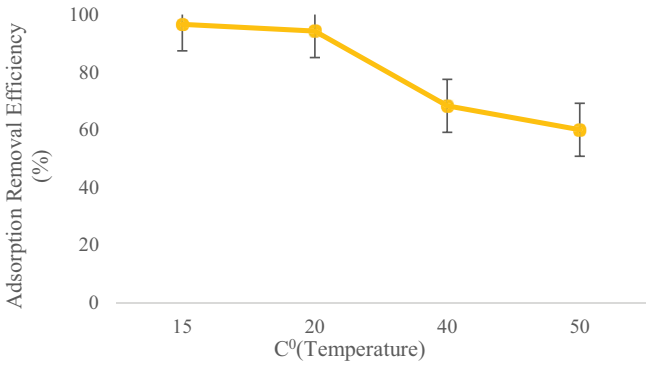

Fig. 12. Temperature effect on the adsorption of *Bitlis pumice* (120 min contact time; 5 mg/L initial concentration; pH: 7).

3.1.9. Adsorption isotherm study

Adsorption isotherms of *Bitlis pumice* on Ni(II) heavy metal were investigated using the Langmuir, Freundlich, Temkin, and Dubinin–Radushkevich isotherm models. The isotherms so obtained are shown in Fig. 13.

Fig. 13 displays direct correlation values of 0.99, 0.90, 0.91, and 0.87, respectively for the Langmuir, Freundlich,

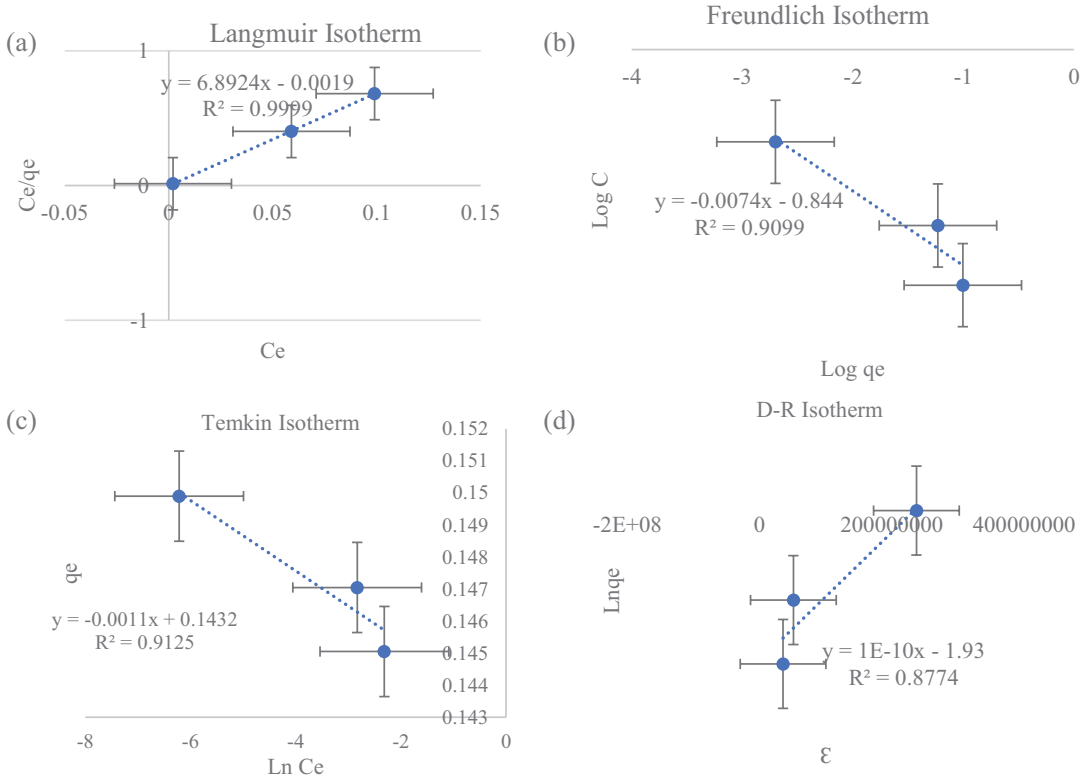

Fig. 13. Isotherm study of the adsorption of *Bitlis pumice* with heavy metal Ni(II). (a) Langmuir, (b) Freundlich, (c) Temkin, and (d) Dubinin–Radushkevich isotherms.

Temkin, and Dubinin–Radushkevich isotherms with regard to *Bitlis pumice*. In terms of these high correlation values, the Langmuir isotherm can be explained by the adsorption processes. This isotherm indicates that there are adsorbing points on the adsorbent surface, and every point is thought to adsorb a molecule with a formed layer of molecular thickness. Every single layer on the surface is coated with Ni(II) heavy metal, where the adsorption adapting to the Langmuir isotherm reaches the highest adsorption capacity within the equilibrium. The Q_0 value, which represents the Langmuir adsorption capacity, and the b value, which indicates the adsorption energy, are given in Table 5 for *Bitlis pumice*. Poly(ethylenimine) functionalized organic–inorganic hybrid silica adsorbent was synthesized using the hydrothermal-assisted surface grafting technique for the removal of Ni(II) ions from aqueous solution, and characterized by FTIR nitrogen adsorption and static adsorption–desorption. It showed that the maximum static adsorption capacity of Ni(II) with regard to poly(ethyleneimine)-functionalized hybrid silica adsorbent using the hydrothermal heating method was 1.6 times that of the conventional heating method. The Langmuir adsorption model was found to be more suitable than the Freundlich and Dubinin–Radushkevich adsorption models [74].

3.1.10. Adsorption kinetic study

The correlation numbers for the pseudo-first-order kinetic and second-order kinetic models were respectively found to be 0.85 and 0.999 according to the data that was obtained because of applying the directly calculated experimental data for the kinetic models. The correlation value is determined as 0.999. Therefore, it is observed that this application fits well with the pseudo-second-order kinetic model. This model is also dependent on the adsorption capacity and rate. It assumes that the Ni(II) concentration remains constant over time and depends on the adsorbent concentration [62]. The kinetic constants are shown in Table 6 and Fig. 14.

3.1.11. Adsorption thermodynamics

Experiments were conducted at different temperatures to determine the adsorption thermodynamics. It was calculated based on the experimental data. By using thermodynamic parameters, the reaction can be explained as either endothermic or exothermic [63]. The $\Delta H°$ value gives informative evidence to determine whether the adsorption process is physical or chemical [63,64]. These parameters are also included in Table 7.

The result of the negative $\Delta G°$ is proof that the adsorption phenomenon occurs spontaneously. It shows higher

Table 7
Thermodynamic constant of Ni(II) removal with *Bitlis pumice*

Temperature (K)	b	$\Delta G°$ (kJ/mol)	$\Delta H°$ (kJ/mol)	$\Delta S°$ (J/mol·K)
288	14.5	–25	56.531	197
293	8.3235	–20		
313	10.789	–18.9		
323	7.5	–21.7		

Table 6
Kinetic constants for *Bitlis pumice*

Bitlis pumice	Pseudo-first-order kinetic model				Pseudo-second-order kinetic model		
	q_{exp} experimental (mg/g)	k_1 (1/min)	q_{exp} Calculated (mg/g)	R^2	k_2 (g/mg·min)	q_{exp} Calculated (mg/g)	R^2
	0.149	0.0541	0.00076	0.85	8.025	0.150	0.999

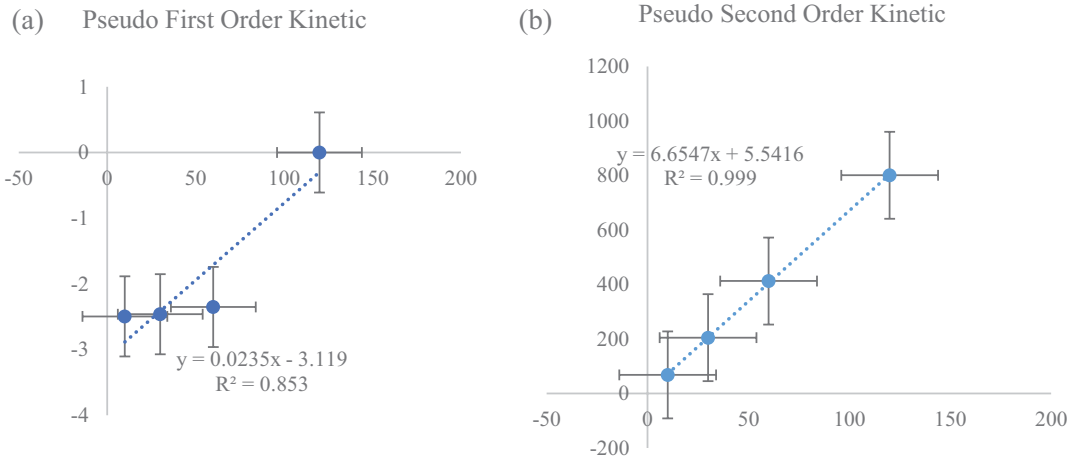

Fig. 14. Adsorption kinetic study. Correlation numbers for the (a) pseudo-first-order kinetic and (b) pseudo-first-order kinetic models.

Table 8
Comparison of Ni(II) removal with other adsorption studies

Adsorbent	Ni(II) (mg/L)	Dose (g/L)	q_{max} (mg/g)	Ni(II) (mg/L)	pH	Time (h)	References
Rice husk ash	100	1	4.84	100	2–10	5	[68]
Manganese dioxide	10–200	10	114.9	10–200	4.5–7.5	24	[69]
Activated carbon	29.3	0.4	34.04	29.3	2.5–8.0	48	[70]
Montmorillonite	50–500	0.5	100%	50–500	3–11	24	[71]
Manganese oxide coated zeolite	100	1	7.9	100	3–8	0.5	[72]
Bitlis pumice	3	1	149.9	3	2–11	2	This study

spontaneity at lower temperatures [73]. A positive $\Delta H°$ value indicated that the adsorption is indeed endothermic and showed that chemical adsorption is the dominant process. In terms of thermodynamics, the adsorption process in the solution phase is quite different from that in the gas phase. In the adsorption process within the solution phase, adsorbate molecules can aggregate, depending on the chemical properties of both adsorbent and adsorbate molecules. Accordingly, the adsorption system involves an endothermic process and needs energy for efficient adsorption [65]. Thus, a positive $\Delta S°$ indicates that there may be a structural differentiation between *Bitlis pumice* and heavy metal Ni(II) forms.

4. Conclusion

The adsorption process is one of the most widely used treatment methods in water and wastewater treatment and is considered the cheapest and most effective technique for removing Ni(II) heavy metal from water. It has become effective in the field of removal due to its simple operation and availability. Moreover, in the last few decades, the adsorption process has been accepted as the primary treatment method for removing pollutants from the environment [66].

Many different adsorbent materials have been used for the adsorption method, which is one of the preferred methods for nickel(II) removal. However, when the data obtained in the series of experiments carried out based on the limited knowledge and research gap for Ni(II) removal in *Bitlis pumice* are examined, it is obvious that this study is a very promising and important study. It will be a pioneering study for different heavy metals and their concentrations in which *Bitlis pumice* will be used as an adsorbent and will encourage other studies. The textural characteristics (i.e., surface area, particle size, pore volume) and Ni(II) adsorption capacity of the *Bitlis pumice* were investigated using different analytical methods. The results obtained revealed that:

(i) The surface area of the *Bitlis pumice* sample was 1.3491 m^2/g (BET model), 1.3719 m^2/g (BJH model), and 16.0137 m^2/g (LA model), whereas the particle size was 4,447 nm. Due to the presence of a negative correlation between particle size and surface area, and a positive correlation between pore volume and surface area, the adsorption capacity of the *Bitlis pumice* stone is more suitable as an absorbent for water purification.
(ii) The pumice particles studied were classified as a mesoporous material with a pore size of 6.30 nm, indicating that pores can selectively separate ions and molecules according to their different sizes.
(iii) The highest removal efficiency of Ni(II) by *Bitlis pumice* stone from artificial water was 99% at an adsorbent dosage of 3 mg/L, pH 7, with a contact time of 120-min according to the Langmuir isotherm model (R^2 = 0.99). This is interpreted chemically by the second-order pseudo-kinetic model (R^2 = 0.99). The Table 7 shows the correlation of thermodynamic fitness as 0.94. The $\Delta H°$ value gives evidence to determine whether the adsorption process is physical or chemical. The result signifies that the Ni(II) adsorption potential of pumice is much higher than is the case with other heavy metals (Table 8).
(iv) All these findings suggest that the mesoporous *Bitlis pumice* stone is a powerful Ni(II) adsorbent material for the purpose of water purification, and a low-cost alternative for further promising future studies on adsorbents. Furthermore, Ni(II) with its high market price, due to its high density (8.9 g/cm^3) relative to pumice (1.00 g/cm^3) can easily be recovered by magnetic (or gravimetric or densimetric) separation to be recycled for economic growth.

Declarations

Ethical approval

The authors have no conflicts of interest to declare that are relevant to the content of this article.

Funding

This study was carried out with the BEBAP 2022.12 project supported by Bitlis Eren University.

Availability of data and materials

Not applicable.

References

[1] N.A.A. Qasem, R.H. Mohammed, D.U. Lawal, Removal of heavy metal ions from wastewater: a comprehensive and critical review, npj Clean Water, 4 (2021) 36, doi: 10.1038/s41545-021-00127-0.

[2] R. Doll, L.G. Morgan, F.E. Speizer, Cancers of the lung and nasal sinuses in nickel workers, Br. J. Cancer, 24 (1970) 623–632.
[3] R. Doll, J.D. Mathews, L.G. Morgan, Cancers of the lung and nasal sinuses in nickel workers: a reassessment of the period of risk, Occup. Environ. Med., 34 (1977) 102–105.
[4] H.M. Shen, Q.F. Zhang, Risk assessment of nickel carcinogenicity and occupational lung cancer, Environ. Health Perspect., 102 (1994) 275–282.
[5] A. Katsnelson, Nickel allergy tracked to a single receptor, Nature, (2010), doi: 10.1038/news.2010.407.
[6] R.L. Prueitt, W. Li, Y.C. Chang, P. Boffetta, J.E. Goodman, Systematic review of the potential respiratory carcinogenicity of metallic nickel in humans, Crit. Rev. Toxicol., 50 (2020) 605–639.
[7] M. Elias, Nickel laterite deposits – geological overview, resources and exploitation, CODES Special Publication, 4 (2002) 205–220.
[8] S.-J. Barnes, P.C. Lightfoot, Economic Geology 100th Anniversary Society of Economic Geologist, 2005, pp. 179–213.
[9] V. Coman, B. Robotin, P. Ilea, Nickel recovery/removal from industrial wastes: a review, Resour. Conserv. Recycl., 73 (2013) 229–238.
[10] C. Quintelas, Z. Rocha, B. Silva, B. Fonseca, H. Figueiredo, T. Tavares, Biosorptive performance of an *Escherichia coli* biofilm supported on zeolite NaY for the removal of Cr(VI), Cd(II), Fe(III) and Ni(II), Chem. Eng. J., 152 (2009) 110–115.
[11] M. Hossein, N. Dalali, A. Karimi, K. Dastanra, Solid phase extraction of copper, nickel, and cobalt in water samples after extraction using surfactant coated alumina modified with indane-1,2,3-trione 1,2-dioxime and determination by flame atomic absorption spectrometry, Turk. J. Chem., 34 (2010) 805–814.
[12] V. Srivastava, C.H. Weng, V.K. Singh, Y.C. Sharma, Adsorption of nickel ions from aqueous solutions by nano alumina: kinetic, mass transfer, and equilibrium studies, J. Chem. Eng. Data, 56 (2011) 1414–1422.
[13] P.K. Pandey, S. Choubey, Y. Verma, M. Pandey, S.S. Kalyan Kamal, K. Chandrashekhar, Biosorptive removal of Ni(II) from wastewater and industrial effluent, Int. J. Environ. Res. Public Health, 4 (2007) 332–339.
[14] M.I. Kandah, J.L. Meunier, Removal of nickel ions from water by multi-walled carbon nanotubes, J. Hazard. Mater., 146 (2007) 283–288.
[15] C. Chen, J. Hu, D. Shao, J. Li, X. Wang, Adsorption behavior of multiwall carbon nanotube/iron oxide magnetic composites for Ni(II) and Sr(II), J. Hazard. Mater., 164 (2009) 923–928.
[16] S.R. Popuri, Y. Vijaya, V.M. Boddu, K. Abburi, Adsorptive removal of copper and nickel ions from water using chitosan coated PVC beads, Bioresour. Technol., 100 (2009) 194–199.
[17] M. Kobya, E. Demirbas, E. Senturk, M. Ince, Adsorption of heavy metal ions from aqueous solutions by activated carbon prepared from apricot stone, Bioresour. Technol., 96 (2005) 1518–1521.
[18] H. Çelebi, G. Gök, O. Gök, Adsorption capability of brewed tea waste in waters containing toxic lead(II), cadmium (II), nickel(II), and zinc(II) heavy metal ions, Sci. Rep., 10 (2020) 17570, doi: 10.1038/s41598-020-74553-4.
[19] M.N. Zafar, R. Nadeem, M.A. Hanif, Biosorption of nickel from protonated rice bran, J. Hazard. Mater., 143 (2007) 478–485.
[20] M. Stevens, B. Batlokwa, Removal of nickel(II) and cobalt(II) from wastewater using vinegar-treated eggshell waste biomass, J. Water Resour. Prot., 9 (2017) 931, doi: 10.4236/jwarp.2017.98062.
[21] D. Sivakumar, J. Nouri, T.M. Modhini, K. Deepalakshmi, Nickel removal from electroplating industry wastewater: a bamboo activated carbon, Global J. Environ. Sci. Manage., 4 (2018) 325–338.
[22] M.K. Öden, E.N. Karasakal, S. Çıldır, Nickel(II) removal from synthetic wastewater by adsorption using waste pea shell, Int. J. Environ. Trends (IJENT), 6 (2022) 10–20.
[23] M. Corral Bobadilla, R. Lostado Lorza, F. Somovilla Gomez, R. Escribano Garcia, Adsorptive of nickel in wastewater by olive stone waste: optimization through multi-response surface methodology using desirability functions, Water, 12 (2020) 1320, doi: 10.3390/w12051320.
[24] I. Timur, B.M. Filiz Senkal, N. Karaaslan, T. Bal, E. Cengiz, M. Yaman, Determination and removing of lead and nickel in water samples by solid phase extraction using a novel Remazol black B-sulfonamide polymeric resin, Curr. Anal. Chem., 7 (2011) 286–295.
[25] J.J. Jacob, R. Varalakshmi, S. Gargi, M.A. Jayasri, K. Suthindhiran, Removal of Cr(III) and Ni(II) from tannery effluent using calcium carbonate coated bacterial magnetosomes, npj Clean Water, 1 (2018) 1, doi: 10.1038/s41545-018-0001-2.
[26] I. Zinicovscaia, N. Yushin, D. Grozdov, K. Vergel, N. Popova, G. Artemiev, A. Safonov, Metal removal from nickel-containing effluents using mineral–organic hybrid adsorbent, Materials, 13 (2020) 4462, doi: 10.3390/ma13194462.
[27] Z. Rahman, Removal of Ni(II) ions from wastewater by raw and modified plant wastes as adsorbents: a review, Iran. J. Chem. Chem. Eng. (IJCCE), 41 (2022) 174–206.
[28] A.H. Mahvi, B. Heibati, A. Mesdaghinia, A.R. Yari, Fluoride adsorption by pumice from aqueous solutions, E-J. Chem., 9 (2012) 1843–1853.
[29] M.R. Samarghandi, M. Zarrabi, M.N. Sepehr, A. Amrane, G.H. Safari, S. Bashiri, Application of acidic treated pumice as an adsorbent for the removal of azo dye from aqueous solutions: kinetic, equilibrium and thermodynamic studies, Iran. J. Environ. Health Sci. Eng., 9 (2012) 1–10.
[30] S.M. Turp, Mn^{2+} and Cu^{2+} adsorption with a natural adsorbent: expanded perlite, Appl. Ecol. Environ. Res., 16 (2018) 5047–5057.
[31] U.A. Guler, M. Sarioglu, Removal of tetracycline from wastewater using pumice stone: equilibrium, kinetic and thermodynamic studies, J. Environ. Health Sci. Eng., 12 (2014) 1–11.
[32] D. Turan, C. Kocahakimoğlu, E. Boyacı, S.C. Sofuoglu, A.E. Eroğlu, Chitosan-immobilized pumice for the removal of As(V) from waters, Water, Air, Soil Pollut., 225 (2014) 1–12.
[33] D. Öztürk, T. Şahan, Design and optimization of Cu(II) adsorption conditions from aqueous solutions by low-cost adsorbent pumice with response surface methodology, Pol. J. Environ. Stud., 24 (2015) 1749–1756.
[34] N. Babakhani, M. Reyahi-Khoram, S. Sobhanardakani, Kinetic study of heavy metal ions removal from aqueous solutions using activated pumice stone, Environ. Health Eng. Manage. J., 3 (2016) 47–53.
[35] D.İ. Çifçi, S. Meriç, A review on pumice for water and wastewater treatment, Desal. Water Treat., 57 (2016) 18131–18143.
[36] S. Indah, D. Helard, Evaluation of iron and manganese-coated pumice from Sungai Pasak, West Sumatera, Indonesia for the removal of Fe(II) and Mn(II) from aqueous solutions, Procedia Environ. Sci., 37 (2017) 556–563.
[37] V. Jonasi, K. Matina, U. Guyo, Removal of Pb(II) and Cd(II) from aqueous solution using alkaline-modified pumice stone powder (PSP): equilibrium, kinetic, and thermodynamic studies, Turk. J. Chem., 41 (2017) 748–759.
[38] A.R. Kul, V. Benek, A. Selçuk, N. Onursal, Using natural stone pumice in van region on adsorption of some textile dyes, J. Turk. Chem. Soc. Sect. A Chem., 4 (2017) 525–536.
[39] B.I. Harman, N.S. Ibrahim, Special Issue of the 7th International Advances in Applied Physics and Materials Science (APMAS 2017) 134/1, 2018, pp. 171–173.
[40] E. Çiçek, The characterization and modeling of cobalt ions adsorption on pumice, Eskisehir Tech. Univ. J. Sci. Technol. A-Appl. Sci. Eng., 22 (2021) 378–383.
[41] B. Tural, E. Ertas, M. Güzel, S. Tural, Effect of structural differences of pumice on synthesis of pumice-supported $n\mathrm{Fe}^0$: removal of Cr(VI) from water, Appl. Water Sci., 11 (2021) 1–11.
[42] S. Alraddadi, H. Assaedi, Physical properties of mesoporous scoria and pumice volcanic rocks, J. Phys. Commun., 5 (2021) 115018, doi: 10.1088/2399-6528/ac3a95.
[43] A.I.M. Ismail, O.I. El-Shafey, M.H.A. Amr, M.S. El-Maghraby, Pumice characteristics and their utilization on the synthesis of mesoporous minerals and on the removal of heavy metals, Int. Scholarly Res. Notices, 2014 (2014) 259379, doi: 10.1155/2014/259379.

[44] S. Indah, D. Helard, B. Primasari, T. Edwin, R.H. Putra, Modification of natural pumice by physical and chemical treatments for removal of zinc ions from aqueous solution, MATEC Web Conf., 276 (2019) 06009, doi: 10.1051/matecconf/201927606009.
[45] M.H. Mahmoudian, A. Azari, A. Jahantigh, M. Sarkhosh, M. Yousefi, S.A. Razavinasab, M. Afsharizadeh, F.M. Shahraji, A.P. Pasandi, A. Zeidabadi, T.I. Bardsiri, M. Ghasemian, Statistical modeling and optimization of dexamethasone adsorption from aqueous solution by Fe_3O_4@NH_2-MIL88B nanorods: isotherm, kinetics, and thermodynamic, Environ. Res., 236 (2023) 116773, doi: 10.1016/j.envres.2023.116773.
[46] E. Türkeş, Master Thesis, 2017. https://tez.yok.gov.tr/UlusalTezMerkezi/tezDetay.jsp?id=iU74sI4VycU6d43b7YCm_A&no=OxievGZ-OuXt4Pqgqzm21w (Access Date: 4.11.2023).
[47] Ş.G. Özkan, G. Tuncer, 4th Industrial Raw Materials Symposium, 2001, pp. 18–19.
[48] M.A. Floriano, A.M. Venezia, G. Deganello, E.C. Svensson, J.H. Root, The structure of pumice by neutron diffraction, J. Appl. Crystallogr., 27 (1994) 271–277.
[49] D. Helard, S. Indah, C.M. Sari, H. Mariesta, The adsorption and regeneration of natural pumice as low-cost adsorbent for nitrate removal from water, J. Geosci. Eng. Environ. Technol., 3 (2018) 86.
[50] A.L. Bush, Construction Materials: Lightweight Aggregates, Encyclopedia of Materials: Science and Technology, 2001, pp. 1550–1558, doi: 10.1016/B0-08-043152-6/00277-1.
[51] M. Sumita, H.U. Schmincke, Impact of volcanism on the evolution of Lake Van I: evolution of explosive volcanism of Nemrut Volcano (Eastern Anatolia) during the past > 400,000 years, Bull. Volcanol., 75 (2013) 1–32.
[52] P.S. Liu, G.F. Chen, General Introduction to Porous Materials, in: Porous Materials, 2014, pp. 1–20.
[53] I.L. Botto, V. Barone, M.E. Canafoglia, E. Rovere, R. Violante, M.J. González, I.B. Schalamuk, Pyroclasts of the first phases of the explosive-effusive PCCVC volcanic eruption: physicochemical analysis, Adv. Mater. Phys. Chem., 5 (2015), doi: 10.4236/ampc.2015.58030.
[54] T. Liu, Z.L. Wang, X. Yan, B. Zhang, Removal of mercury(II) and chromium(VI) from wastewater using a new and effective composite: pumice-supported nanoscale zero-valent iron, Chem. Eng. J., 245 (2014) 34–40.
[55] M. Thommes, K. Kaneko, A.V. Neimark, J.P. Olivier, F. Rodriguez-Reinoso, J. Rouquerol, K.S. Sing, Physisorption of gases, with special reference to the evaluation of surface area and pore size distribution (IUPAC Technical Report), Pure Appl. Chem., 87 (2015) 1051–1069.
[56] H. Kayakökü, M. Doğru, Assessment of radioactivity and heavy metal contents in surface water samples from Van Lake, Turkey, Arabian J. Geosci., 14 (2021) 1093, doi: 10.1007/s12517-021-07397-5.
[57] D.İ. Çifçi, S.M. Pagano, Comparison of pumice-based adsorbents for lithium adsorption in synthetic aqueous, Fırat Univ. J. Eng. Sci., 33 (2021) 185–192.
[58] M.H. Dehghani, M. Sarmadi, M.R. Alipour, D. Sanaei, H. Abdolmaleki, S. Agarwal, V.K. Gupta, Investigating the equilibrium and adsorption kinetics for the removal of Ni(II) ions from aqueous solutions using adsorbents prepared from the modified waste newspapers: a low-cost and available adsorbent, Microchem. J., 146 (2019) 1043–1053.
[59] S. Maleki, A. Karimi-Jashni, Effect of ball milling process on the structure of local clay and its adsorption performance for Ni(II) removal, Appl. Clay Sci., 137 (2017) 213–224.
[60] E. Malkoc, Y. Nuhoglu, Removal of Ni(II) ions from aqueous solutions using waste of tea factory: adsorption on a fixed-bed column, J. Hazard. Mater., 135 (2006) 328–336.
[61] S. Malamis, E. Katsou, A review on zinc and nickel adsorption on natural and modified zeolite, bentonite and vermiculite: examination of process parameters, kinetics and isotherms, J. Hazard. Mater., 252 (2013) 428–461.
[62] F.E. Erkurt, B. Balcı, Investigation of adsorption of Reactive Black 5 dye onto activated carbon by using kinetic and adsorption models, Çukurova University, J. Fac. Eng. Archit., 30 (2015) 257–270.
[63] E. Koohzad, D. Jafari, H. Esmaeili, Adsorption of lead and arsenic ions from aqueous solution by activated carbon prepared from tamarix leaves, Chem. Select, 4 (2019) 12356–12367.
[64] A. Çiçekçi, B. Dönmez, E. Kavcı, Ö. Laçin, Adsorption isotherms and thermodynamics on peach kernel peel of malahit green, Sinop Univ. J. Nat. Sci., 5 (2020) 103–111.
[65] D.S. Qais, M.N. Islam, M.H.D. Othman, H.E. Mahmud, M.E. Quayum, M.A. Islam, A. Habib, Nano-zinc oxide fibers: synthesis, characterization, adsorption of Acid Blue 92 dye, isotherms, thermodynamics and kinetics, Emerg. Contam., 9 (2023) 100224, doi: 10.1016/j.emcon.2023.100224.
[66] S.Y. Hashemi, A. Azari, M. Raeesi, K. Yaghmaeian, Application of response surface methodology (RSM) in optimisation of fluoride removal by magnetic chitosan/graphene oxide composite: kinetics and isotherm study, Int. J. Environ. Anal. Chem., 103 (2023) 5368–5386.
[67] M. Yeganeh, A. Azari, H.R. Sobhi, M. Farzadkia, A. Esrafili, M. Gholami, A comprehensive systematic review and meta-analysis on the extraction of pesticide by various solid phase-based separation methods: a case study of malathion, Int. J. Environ. Anal. Chem., 103 (2023) 1068–1085.
[68] V.C. Srivastava, I.D. Mall, I.M. Mishra, Competitive adsorption of cadmium(II) and nickel(II) metal ions from aqueous solution onto rice husk ash, Chem. Eng. Process. Process Intensif., 48 (2009) 370–379.
[69] D.C. Ong, S.M.B. Pingul-Ong, C.C. Kan, M.D.G. de Luna, Removal of nickel ions from aqueous solutions by manganese dioxide derived from groundwater treatment sludge, J. Cleaner Prod., 190 (2018) 443–451.
[70] H. Liu, X. Wang, G. Zhai, J. Zhang, C. Zhang, N. Bao, C. Cheng, Preparation of activated carbon from lotus stalks with the mixture of phosphoric acid and pentaerythritol impregnation and its application for Ni(II) sorption, Chem. Eng. J., 209 (2012) 155–162.
[71] M.M. Akafia, T.J. Reich, C.M. Koretsky, Assessing Cd, Co, Cu, Ni, and Pb sorption on montmorillonite using surface complexation models, Appl. Geochem., 26 (2011) S154–S157.
[72] M. Irannajad, H.K. Haghighi, Removal of Co^{2+}, Ni^{2+}, and Pb^{2+} by manganese oxide-coated zeolite: equilibrium, thermodynamics, and kinetics studies, Clays Clay Miner., 65 (2017) 52–62.
[73] D. Hao, Y.X. Song, Y. Zhang, H.T. Fan, Nanocomposites of reduced graphene oxide with pure monoclinic-ZrO_2 and pure tetragonal-ZrO_2 for selective adsorptive removal of oxytetracycline, Appl. Surf. Sci., 543 (2021) 148810, doi: 10.1016/j.apsusc.2020.148810.
[74] L. He, B.B. Wang, D.D. Liu, K.S. Qian, H.B. Xu, Poly(ethyleneimine) functionalized organic-inorganic hybrid silica by hydrothermal assisted surface grafting method for removal of nickel(II), Korean J. Chem. Eng., 31 (2014) 343–349.